Supporting Information

Enhanced excitonic luminescence and fast scintillation potential in Sr^{2+}-activated $CsPbCl_3$ single crystals

Andrii Pushak[1], Oleksandr Pidhornyi[1], Yaroslav Chornodolskyy[1], Taras Malyi[1], Taras Demkiv[1*], Oleh Antonyak[1], Volodymyr Stakhura[1], Volodymyr Salapak[2], Roman Gamernyk[1], Oleh Bovgyra[1], Anatoliy Zelinskiy[1], Yevheniia Smortsova[3], Aleksei Kotlov[3], Anatoliy Voloshinovskii[1]

[1]*Ivan Franko National University of Lviv, 1 Universytetska Str., 79000, Lviv, Ukraine*
[2]*Ukrainian National Forestry University, 103 Gen. Chuprynky St., 79057, Lviv, Ukraine*
[3]*Deutsches Elektronen-Synchrotron DESY, Notkestr. 85, 22607 Hamburg, Germany*

*Corresponding author: taras.demkiv@lnu.edu.ua

1. Elemental composition

The elemental composition of the samples was determined using a Tescan Vega3 LMU scanning electron microscope equipped with an Oxford Instruments Aztec ONE energy-dispersive X-ray spectrometer and an X-MaxN20 detector. The samples were mounted on a graphitized conductive film. Surface scanning was performed with an electron beam generated by an electron gun (W-thermocathode, 20–30 kV). The results are presented in Fig. S1 and Table S1.

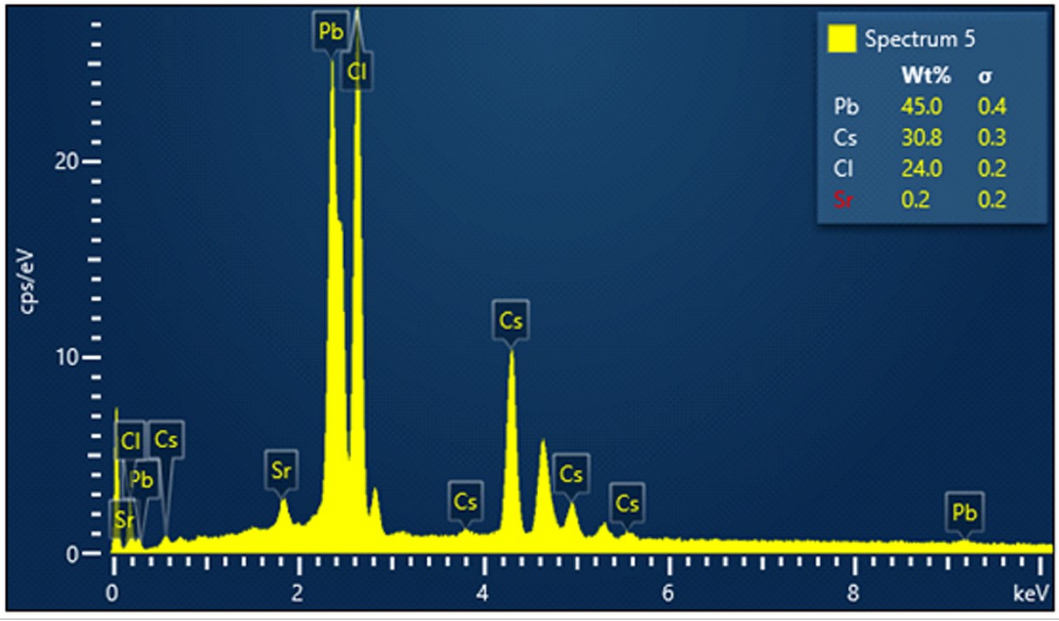

Figure S1. Energy-dispersive X-ray (EDX) spectrum of the $CsPbCl_3$:Sr(1 mol%) crystal.

Table S1. Elemental composition of the $CsPbCl_3$:Sr samples determined by energy-dispersive X-ray spectroscopy.

Concentration in raw material	**Concentration in crystal**					
Sr, mol%	**Cs, wt%**	**Pb, wt%**	**3Cl, wt%**	**Sr, wt%**	**Total**	**Sr, mol%**
0,5	29.62±0.12	46.32±0.15	23.95±0.09	0.11±0.06	100	0,47
1	30.80±0.12	45.00±0.15	24.00±0.09	0.20±0.06	100	0,85
5	30.50±0.12	45.07±0.15	24.24±0.09	1.15±0.06	100	4,74

2. Energy band structure of the $CsPbCl_3$ and the $CsPbCl_3$:Sr crystals

All theoretical calculations are completed using the density functional theory (DFT) implemented in the CASTEP package based on pseudopotential plane-wave methods [1]. We apply the Perdew-Burke-Ernzerhof (PBE) parametrization for generalized gradient approximation (GGA) to describe the exchange-correlation

functional. After convergence tests, the plane-wave basis set cut-off energy was set as 450 eV; the convergence tolerance for energy was set as 5×10^{-6} eV/atom, and the tolerance for maximum force was 0.01 eV/Å. A 2×2×2 supercell was used to simulate the substitutional doping $CsPbCl_3$ system. First, we provide geometry optimization of undoped $CsPbCl_3$ crystal using the effective Broyden-Fletcher-Goldfarb-Shanno algorithm. Next, we substituted one Pb atom in the supercell with a Sr atom, and the optimization procedure was repeated using the same algorithm. The interactions between the atomic core and valence electrons were described using ultrasoft pseudopotentials. The Monkhorst-Pack scheme of 6×6×6 k-point sampling for integration on the first Brillouin zone was used. For a more accurate description of electronic spectra, Hubbard correction was applied to GGA, the so-called GGA+U method. The Hubbard U parameter was chosen at 5 eV and applied to Cl p-states like in the proposed scheme [2].

Fig. S2 presents the band structure of $CsPbCl_3$ and Sr-doped $CsPbCl_3$ calculated using GGA+U method.

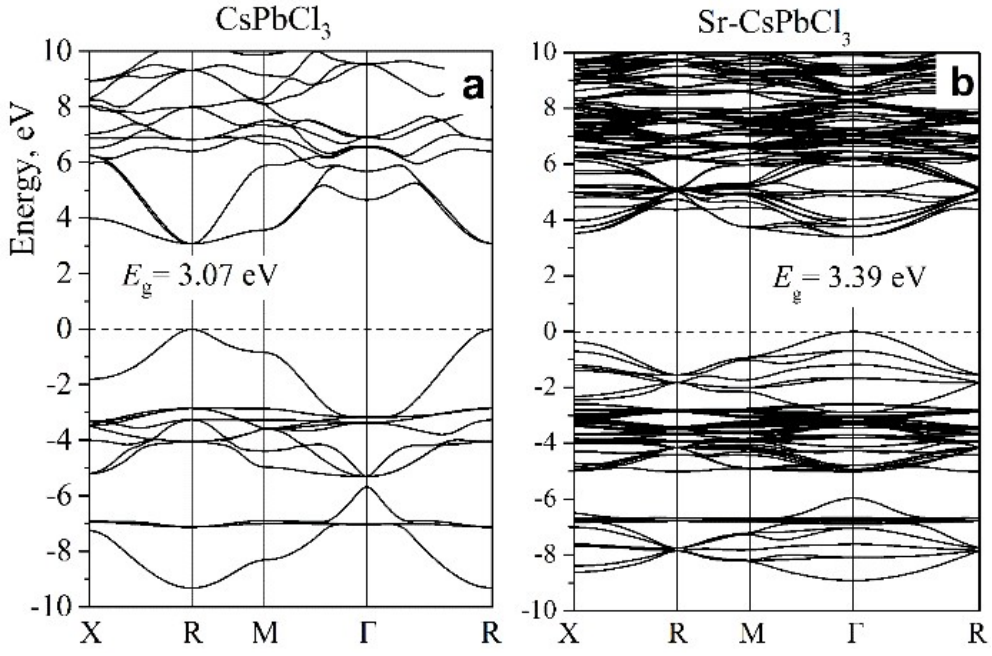

Figure S2. The band structure of $CsPbCl_3$ (a) and Sr-doped $CsPbCl_3$ (b) calculated using the GGA+U method. The Fermi level depicted a horizontal dashed line at 0 eV.

The calculation results indicate a direct band gap at the R-point for pristine $CsPbCl_3$ (see Fig. S2 (a)). The introduction of the Sr atom significantly modifies the electronic structure of the doped $CsPbCl_3$ crystal. As shown in Fig. S2 (b), the band

structure of Sr-doped $CsPbCl_3$ exhibits noticeable changes when compared to the undoped material. The most significant modification is the shift of electronic states forming the direct band gap from the high-symmetry point R to the Γ point. The band gap of the Sr-doped $CsPbCl_3$ system was calculated to be 3.39 eV. This value represents a notable increase compared to the band gap of the undoped perovskite, indicating a significant effect of Sr doping on the material's electronic properties.

To elucidate the nature of the electronic properties of $CsPbCl_3$ perovskite, the total density of state and partial density of state were calculated. Fig. S3 shows the DOS and PDOS obtained using the GGA + U method.

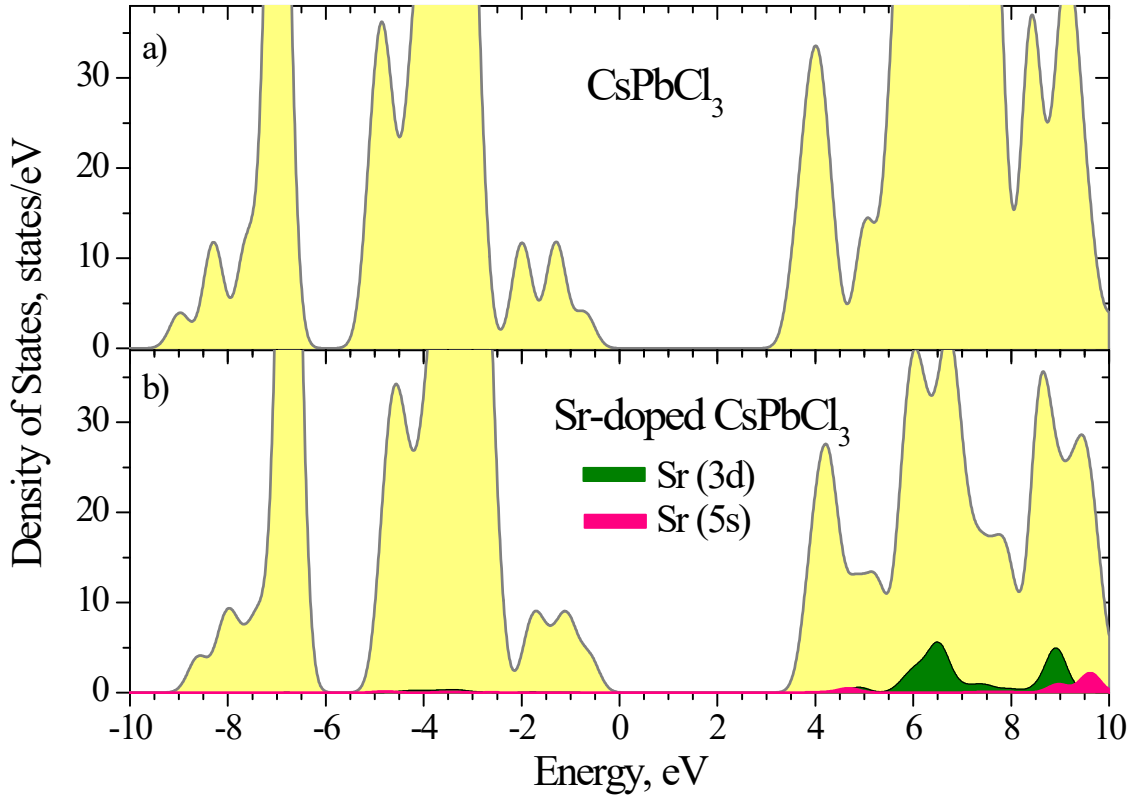

Figure S3. Total and Partial density of states of the pristine and the strontium doped $CsPbCl_3$ crystals. a) Total density of states of the pristine $CsPbCl_3$ crystal. b) Total density of states of the Sr-doped $CsPbCl_3$ crystal and partial density of states of Sr 3d and Sr 5s orbitals. Results based on 2×2×2 supercell.

The analysis of the DOS provides insights into the overall distribution of electronic states across energy levels. At the same time, the PDOS helps to distinguish the specific contributions from different atomic species and their respective orbitals.

Compared to the undoped perovskite (Fig. S3(a)), the main valence band overall structure remains unchanged, indicating that the fundamental electronic framework is

preserved despite the introduction of the dopant. However, the most significant effect of the Sr atom is the presence of additional *d*- and *s*-states into the electronic structure. These *d*-states appear in the conduction band, particularly within the 5 to 10 eV energy range. At the same time, the s-states of Sr make a minor contribution.

3. Impurity formation energies in Sr-doped $CsPbCl_3$ crystal

To confirm the relative stability of the Sr-doped $CsPbCl_3$, we calculated the impurity formation energies (E_f) using the following expression:

$$E_f = E_{doped} + E_X - E_{pure} - E_{Sr}, \quad (1)$$

where E_{doped} is the total energy of the Sr-doped $CsPbCl_3$ crystal, E_X is the total energy of the removed atom, E_{pure} is the total energy of pure $CsPbCl_3$, and E_{Sr} is the total energy of the isolated Sr atom. A negative E_f value indicates a stable perovskite. Our calculations included three different dopant sites of the Sr atom: Sr atom replaced Cs atom, Sr atom replaced Pb atom, and Sr atom replaced Cl atom. The results obtained show that when a strontium atom replaces a cesium atom, the formation energy becomes 1.44 eV. In the case of replacing the Pb atom with the Sr atom, E_f is −1.74 eV, and for the Sr atom on the Cl site, the formation energy is 5.71 eV. In general, a positive formation energy suggests that the atomic substitution approach is unlikely to be feasible for experimental preparation, whereas a negative formation energy implies that Sr can partially substitute Pb^{2+} ions in the perovskite lattice. Additionally, the Sr–Cl bond lengths are 2.859 Å, meanwhile the Pb–Cl bond lengths range from 2.861 to 2.863 Å. This indicates that the inclusion of the Sr atom in the perovskite structure leads to the formation of a stronger bond than the Pb–Cl bond.

4. Exciton binding energy

Based on the band structure calculations presented in SI, Chapter 2, the next stage of our investigation involved calculating the exciton binding energy. To evaluate the impact of doping on the mobility of charge carriers, we calculated the effective masses of electrons (m_e*) and holes (m_h*) in both the undoped and the Sr-doped $CsPbCl_3$. The effective masses were determined from the band dispersion at high symmetric points that forming bandgap using the following equation:

$$\frac{1}{m^*} = \frac{1}{\hbar^2}\frac{\partial^2 E(k)}{\partial^2 k}, \quad (2)$$

where $\hbar$ is the reduced Planck constant, k is the wave vector along different directions, and $E(k)$ is the energy dispersion function.

The exciton binding energy (E_b) was calculated using the obtained electron and hole effective masses, based on the Wannier−Mott exciton model, using the following equation:

$$E_b = 13.6\frac{\mu}{\varepsilon_{eff}^2} \quad (3)$$

where μ is the reduced effective mass of the electron-hole pair ($1/\mu = 1/m_e^* + 1/m_h^*$), ε_{eff} is the effective dielectric permittivity (the high-frequency dielectric constant) calculated by using density functional perturbation theory, and 13.6 eV is the Rydberg energy or the ionization energy of a ground-state H atom.

Table S2. Calculated effective mass of electron (m_e^*) and hole (m_h^*), reduced mass (μ), static dielectric permittivity (ε_{eff}), and exciton binding energy (E_b) of $CsPbCl_3$ and Sr-doped $CsPbCl_3$.

Compound	m_e^* (m_0)	m_h^* (m_0)	μ (m_0)	ε_{eff}	E_b (meV)
$CsPbCl_3$	0.968	0.257	0.203	6.316	69.2
Sr-doped $CsPbCl_3$	0.257	0.130	0.086	6.185	30.6

The calculated values of the effective dielectric constant and the reduced effective mass are summarized in Table S2. In Sr-doped $CsPbCl_3$, the effective dielectric permittivity (ε_{eff}) shows a slight decrease of about 0.2 relative to the undoped crystal. The variations in effective mass, combined with the reduced dielectric constant, lead to a lower exciton binding energy in the Sr-doped compound (see Table S2).

5. Influence of strontium doping on the formation energy of chlorine vacancies

We investigated the effect of Sr-doping on the structural stability of the perovskite by calculating the Cl vacancy (V_{Cl}) formation energy. The formation energy of chlorine vacancies in $CsPbCl_3$ was calculated within density functional theory using the CASTEP code. A supercell model (2×2×2) of the cubic perovskite structure was constructed, and chlorine vacancies were introduced by removing a single Cl atom, followed by full geometry optimization. For Sr-doped systems, a Pb atom was substituted by Sr^{2+}, and the Cl vacancy was created at various positions relative to the dopant to analyse coordination effects.

The vacancy formation energy (E_{vac}) was calculated using the following expression:

$$E_{vac} = E_{s-vac} + E_{Cl} - E_s, \quad (4)$$

where E_s is the total energy of supercell $CsPbCl_3$ without a vacancy, $E_{s\text{-}vac}$ is that of the supercell with a vacancy, and E_{Cl} is 1/2 of the total energy of Cl_2 molecule in a gas phase.

The study of perovskite stability in relation to point defects is critical, given their substantial influence on electronic and optical properties. Computational results show that the formation energy for a chlorine vacancy (E_{vac}) is 2.79 eV for pristine $CsPbCl_3$ and 5.46-6.68 eV for Sr-doped $CsPbCl_3$ (depending on the position of the chlorine vacancy relative to the Sr dopant ion, where higher formation energy is characteristic of chlorine vacancies located closer to the Sr). The positive values confirm that vacancy formation is an endothermic process for both materials.

Our results on the formation energies of chlorine vacancies are consistent with the data reported in reference [3]. Specifically, the formation energy of V_{Cl} in the pristine crystal is 3.15 eV, while in the case of Ni, Co, and Fe doping, it is 4.78, 5.63, and 6.06 eV, respectively.

The observation that the vacancy formation energy is higher in the Sr-doped perovskite than in the undoped structure is highly significant. This result implies that introducing Sr as a dopant makes the formation of the Cl vacancy (V_{Cl}) less thermodynamically favourable. This finding can be directly interpreted as the Sr dopant stabilizing the perovskite structure. Essentially, the presence of Sr atoms enhances the

overall structural integrity of the lattice, thereby reducing the likelihood of point defects occurring.

The elevated energy required to form vacancies in the doped structure reveals a significant finding: Sr introduction does more than just alter electronic properties – it also leads to improved structural stability in the perovskite.

6. Luminescent parameters of the $CsPbCl_3$ and the $CsPbCl_3$:Sr(1 mol%)

Fig. S4 shows the luminescence spectra of the $CsPbCl_3$ and the $CsPbCl_3$:Sr (1 mol%) at 10 K and 80 K. From this figure, it is evident that at 80 K the luminescence intensity of the doped crystal remains higher than that of the pristine sample, and the emission bands in the short-wavelength region of the spectrum experience less quenching for the $CsPbCl_3$:Sr (1 mol%).

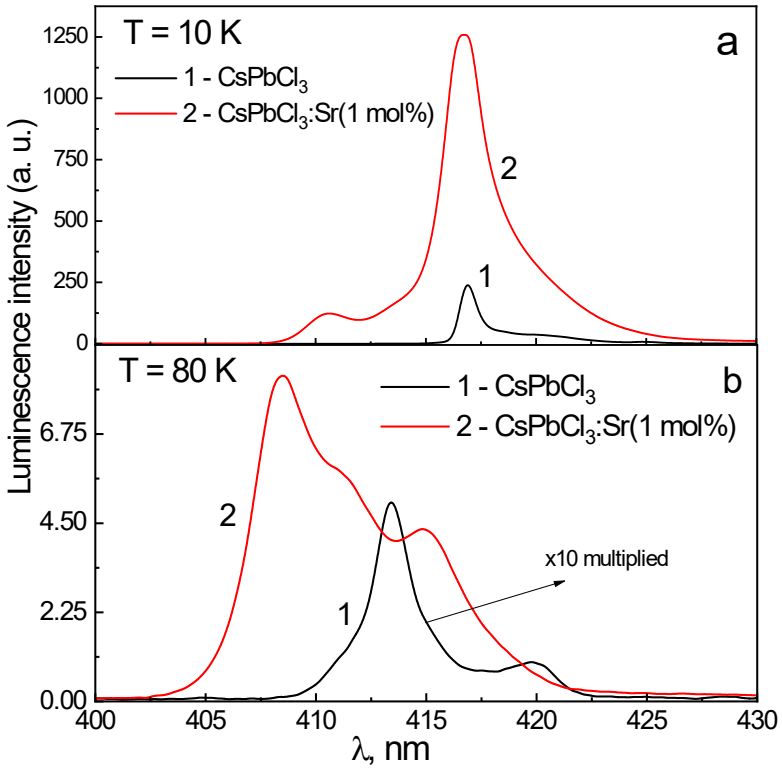

Figure S4. Luminescence spectra of the $CsPbCl_3$ (curve 1) and the $CsPbCl_3$:Sr (1 mol%) (curve 2) at T = 10 K (a) and T = 80 K (b).

7. Luminescence decay kinetics of the $CsPbCl_3$ and $CsPbCl_3$:Sr(1 mol%)

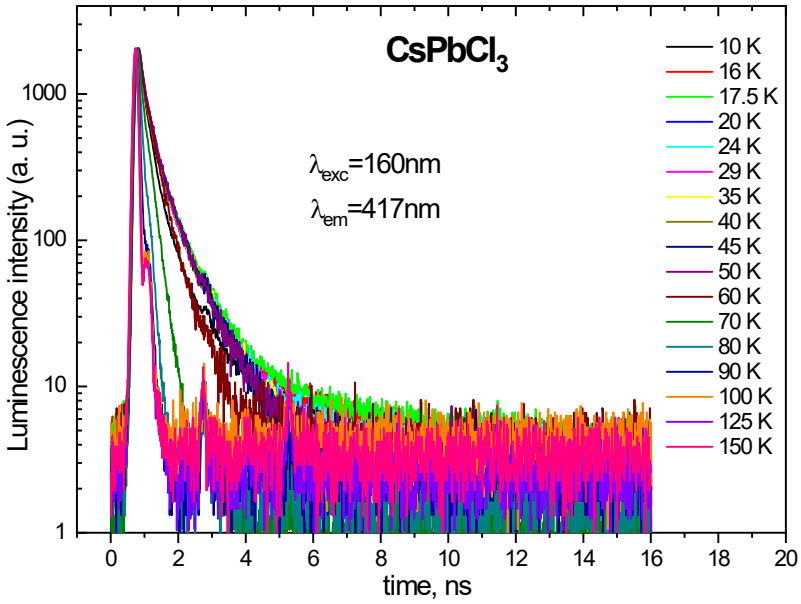

Figure S5. Luminescence decay curves of the 417 nm luminescence band of the $CsPbCl_3$ single crystal at different temperatures under excitation with light of $h\nu_{exc}$ = 7.7 eV (λ_{exc} = 160 nm).

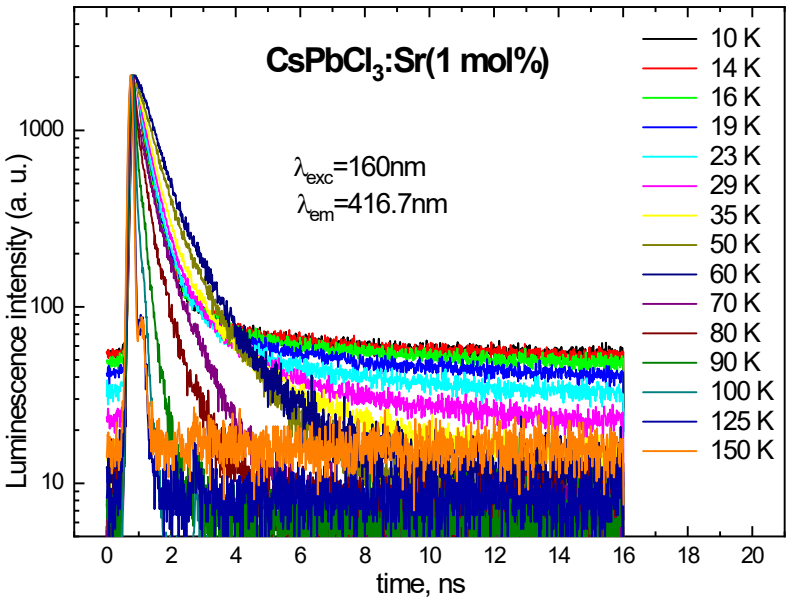

Figure S6. Luminescence decay curves of the 416.7 nm luminescence band of the $CsPbCl_3$:Sr (1 mol%) single crystal at different temperatures under excitation with light of $h\nu_{exc}$ = 7.7 eV (λ_{exc} = 160 nm).

References

1. M. D. Segall, P. J. D. Lindan, M. J. Probert, C. J. Pickard, P. J. Hasnip, S. J. Clark, M. C. Payne, *First-principles simulation: ideas, illustrations and the CASTEP code, J. Phys. Condens. Matter,* 2002, 14, 2717.
2. E. Welch, L. Scolfaro, A. Zakhidov, *Density functional theory + U modeling of polarons in organohalide lead perovskites, AIP ADVANCES*, 2016, 6, 125037.
3. H. Jiang, Y. Zhao, F. Liu, Y. Yan, Y. Ma, H. Bao, Z. Wu, W.-Y. Cong, Y.-B. Lu, *Mono- and Co-Doped Mn-Doped $CsPbCl_3$ Perovskites with Enhanced Doping Efficiency and Photoluminescent Performance, Materials* **16**, 5545 (2023).